ADVANCED ELECTRONIC MATERIALS Open Access
www.advelectronicmat.de

A Giant Tunable Piezoelectric Performance in Two-dimensional In_2Se_3 via Interface Engineering

Shuoguo Yuan, Yiming Zhang, Minzhi Dai, Yancong Chen, Haiyan Yu, Zengsheng Ma, Weng Fu Io, Xin Luo,* Pengfei Hou,* and Jianhua Hao**

Two-dimensional (2D) layered piezoelectric materials have attracted enormous interest, which leads to wide applications in stretchable electronic, energy and biomedicine. The piezoelectric properties of 2D materials are mainly modulated by strain, thickness, defect engineering and stacked structure. However, the tunability of piezoelectric properties is typically limited by the small variation within one order of magnitude. It is challenging to obtain high tunable piezoelectric properties of 2D materials. Here, this study reports that the out-of-plane piezoelectric properties of 2D van der Waals In_2Se_3 are significantly manipulated using interface engineering. The variation value of piezoelectric properties is above two orders of magnitude, giving rise to the highest variation value in the 2D piezoelectric materials system. In particular, the 2D materials In_2Se_3 can be directly fabricated onto silicon substrate, which suggests its compatibility with the state-of-the-art silicon semiconductor technology. Combining the experimental and computational results, this study reveals that the ultrahigh tunable piezoelectric properties result from the interface charge transfer effect. The work opens the door to design and modulate the unprecedented applications of atomic-scale smart and multifunctional devices.

1. Introduction

Piezoelectricity in two-dimensional (2D) materials has attracted much interest owing to wide range of promising applications in stretchable electronics, actuators, piezocatalysis, piezotronics and biomedicine.[1–7] Typically, the 2D layered materials, such as MoS_2,[8,9] WSe_2,[10] SnS,[11] and MXene,[12] have in-plane piezoelectricity due to the lack of inversion symmetry along the in-plane direction. In particular, in a number of reported 2D piezoelectric materials, such as MoS_2, the out-of-plane piezoelectric responses are commonly limited to odd-numbered layers, and their magnitude would gradually reduce or even vanish with increasing the number of layers. Additionally, the extensive applications of in-plane 2D piezoelectric materials are constrained when integrating with standard semiconductor substrates like silicon, because the modulation of stress needs to stretch the substrates to generate the in-plane strain. Recently, out-of-plane piezoelectricity in the 2D material family has been reported in In_2Se_3, MoSSe, $CuInP_2S_6$, and $NbOI_2$.[13–16] However, the variation of piezoelectric properties is typically within one order of magnitude with low tunable piezoelectric response.[17–21]

In this study, we report that a giant out-of-plane tunable piezoelectric response can be achieved in In_2Se_3 via interface engineering, which exhibits the highest variation value in the 2D

S. Yuan, H. Yu
Faculty of Materials Science and Chemistry
China University of Geosciences
Wuhan 430074, China
E-mail: yuanshuoguo@cug.edu.cn
Y. Zhang, Z. Ma, P. Hou
School of Materials Science and Engineering
Xiangtan University
Xiangtan 411105, China
E-mail: houpf@xtu.edu.cn
M. Dai, Y. Chen, X. Luo
School of Physics
Sun Yat-Sen University
Guangzhou 510275, China
E-mail: luox77@mail.sysu.edu.cn
W. F. Io, J. Hao
Department of Applied Physics
The Hong Kong Polytechnic University
Hung Hom, Hong Kong China
E-mail: jh.hao@polyu.edu.hk

The ORCID identification number(s) for the author(s) of this article can be found under https://doi.org/10.1002/aelm.202300741

DOI: 10.1002/aelm.202300741

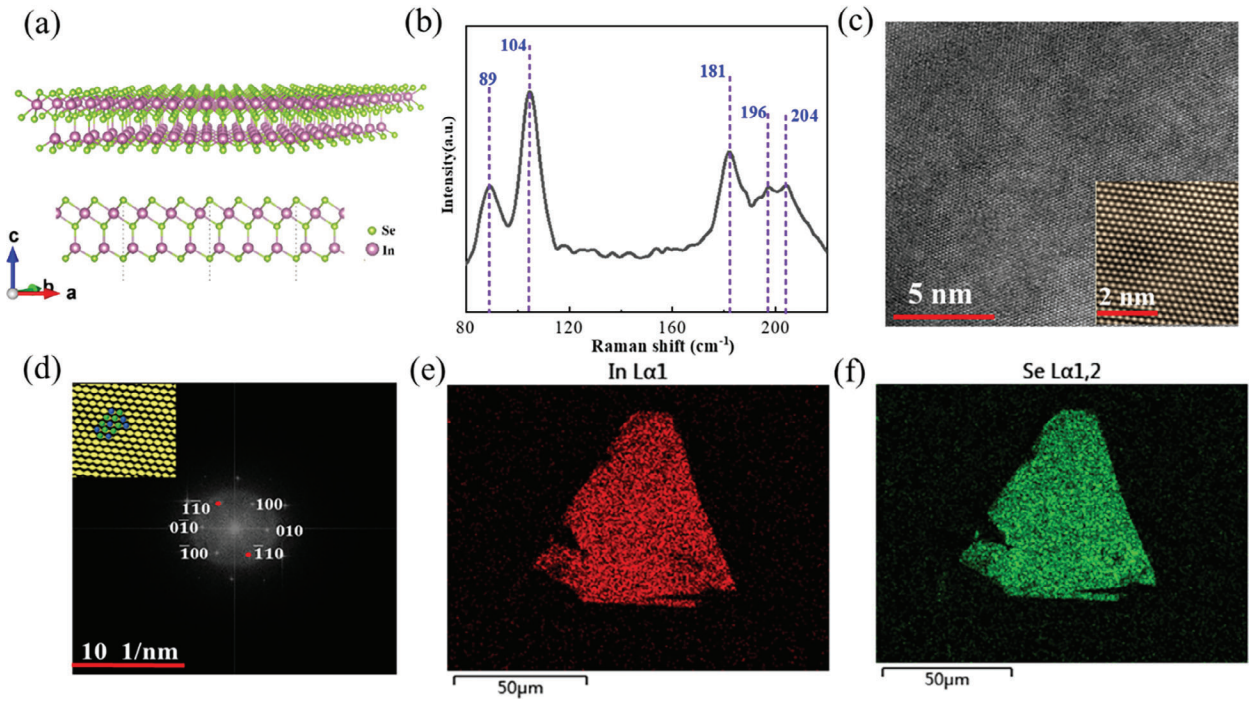

Figure 1. Structural characterizations of α-In_2Se_3. a) Atomic structure of In_2Se_3. b) Raman spectrum of In_2Se_3. c) High-resolution TEM image of In_2Se_3 and the inset shows large-scale image. d) SAED pattern of In_2Se_3 and the inset shows the atomic structure. e,f) Elemental mapping of In and Se.

piezoelectric material system. In addition, the 2D piezoelectric material In_2Se_3 is directly fabricated onto a silicon substrate, which can easily integrate with the silicon-based technology. Furthermore, we reveal that the physical mechanism of the ultrahigh tunable piezoelectric properties is related to the charge transfer of the interface. The significant tunable piezoelectric response of 2D materials via interface modulation will lead to unexpected applications in atomic-scale smart and multifunctional coupling devices.

2. Results and Discussion

The 2D material In_2Se_3 possesses different phases due to the stacking sequence of the layer. Among these phases of In_2Se_3, the α phase In_2Se_3 exhibits strong out-of-plane piezoelectric properties. A single α-In_2Se_3 layer includes the atomic structure stacked in the order of Se-In-Se-In-Se. **Figure** 1a shows the atomic structure of the α-In_2Se_3. The middle layer of the Se atom shifted off-centre brings the absence of mirror symmetry, giving rise to vertical piezoelectricity. To verify the phase of In_2Se_3, Raman spectroscopy is employed to characterize the structure by the characteristic Raman vibration modes. Figure 1b reveals the Raman spectrum of In_2Se_3 samples, the α-In_2Se_3 displays three main Raman peaks at 181, 196 and 204 cm^{-1}, which are associated with the A(LO) mode. Furthermore, α-In_2Se_3 also includes two more Raman peaks below 150 cm^{-1}, which are located close to 89 and 104 cm^{-1}, corresponding to the E mode and A(LO+TO) modes.[13] To characterize the structure of In_2Se_3 samples, the structural characterization of In_2Se_3 was characterized through transmission electron microscopy (TEM). Figure 1c displays TEM images of In_2Se_3 while Figure 1d presents the selected area electron diffraction (SAED) pattern of In_2Se_3. The diffraction pattern with sixfold rotational symmetry supports that In_2Se_3 has the hexagonal symmetry. Through elemental mapping and energy dispersive spectroscopy (Figure 1e,f; Figure S1, Supporting Information), the atomic ratio of In/Se is verified, and the results indicate that the atomic ratio of In/Se is ~2/3.

Typically, the piezoelectric properties of 2D materials are measured through piezoresponse force microscopy (PFM). Based on the measurement of the converse piezoelectric response, the samples are deformed under an applied vertical electrical field, which causes the amplitude variation in the PFM imaging. The samples piezoelectric properties are usually estimated using the piezoelectric coefficient d_{33}. A background subtraction method is used to quantify the genuine piezoelectric response and reduce the contribution from non-electromechanical influences. As shown in **Figure** 2, the piezoelectric response in In_2Se_3 exhibits a distinct colour contrast. Because the substrate does not provide a visible contrast under the same experimental conditions, this apparent colour contrast does not arise from topographical, mechanical, or electrochemical artefacts. PFM amplitude images exhibit a distinct piezoelectric response due to the non-centrosymmetric structure, resulting in out-of-plane piezoelectricity in In_2Se_3. As the drive voltage increases, the vertical PFM amplitude of In_2Se_3 increases (Figure S2, Supporting Information). The piezoelectric coefficient d_{33} can be obtained from the relationship between the amplitude and drive voltage using $A = d_{eff}VQ$, where A, d_{eff}, V, and Q denote the amplitude, effective piezoelectric coefficient, drive voltage, and quality factor, respectively. When the indentation of the PFM tip make the contact section with the sample less than the tip radius of ~25 nm, the value of piezoelectric coefficient d_{33} is approximately twofold than d_{eff}.[13] To quantitatively determine the vertical piezoelectric coefficient d_{33} of In_2Se_3 on the Pt substrate, the relationship between

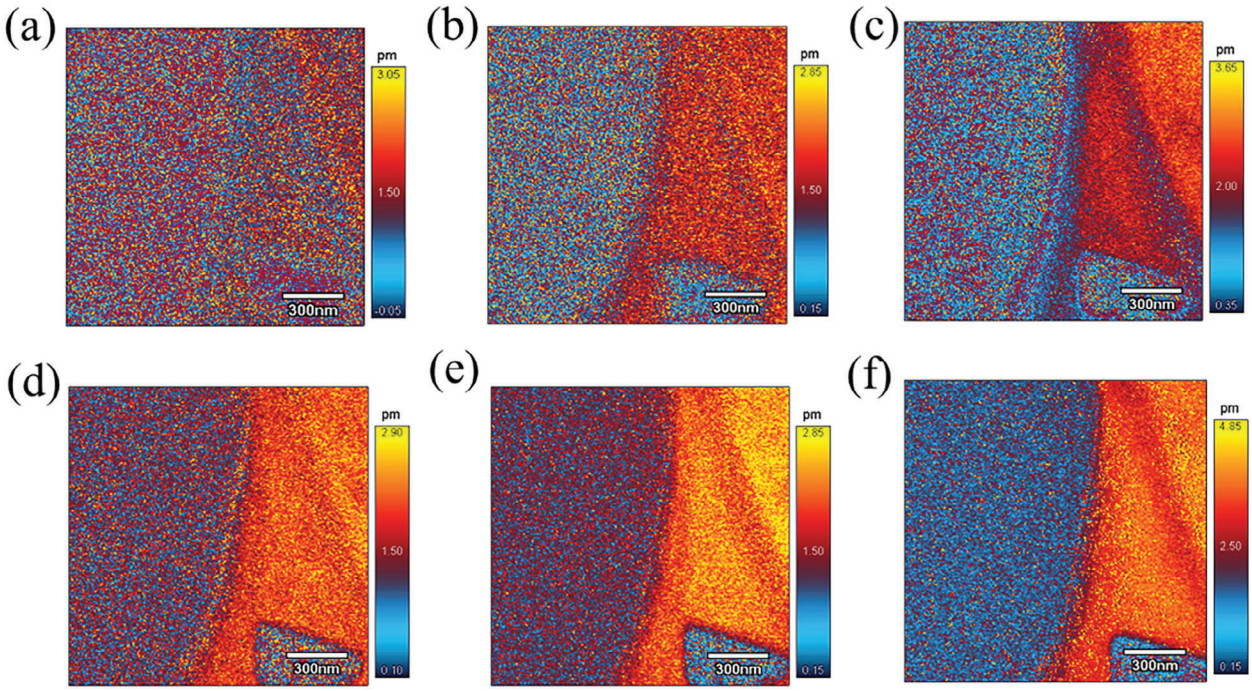

Figure 2. Vertical piezoelectricity of α-In_2Se_3 onto Pt substrate. PFM amplitude images of In_2Se_3 with different drive voltages a) 0.5 V; b) 1 V; c) 1.5 V; d) 2 V; e) 2.5 V; f) 3 V; scale bar, 0.3 μm).

the piezoelectric amplitude and applied drive voltage is presented in Figure S3 (Supporting Information). Additionally, PFM amplitude images of different In_2Se_3 samples fabricated onto Pt substrate substrates are exhibited in Figure S4 (Supporting Information), which exhibits similar results. Moreover, the PFM amplitude images of In_2Se_3 fabricated onto *p*-type Si and *n*-type Si substrates are shown in Figures S5–S11 (Supporting Information).

To demonstrate the vertical piezoelectric properties controlled by the interface effect, the thickness-dependent vertical piezoelectric properties d_{33} of In_2Se_3 with different interface environments such as Pt, *p*-type Si, and *n*-type Si substrates are shown in **Figure 3**. The piezoelectric coefficient d_{33} of In_2Se_3 enhances with an increasing thickness, and the piezoelectric coefficient d_{33} sequentially increases to a relatively saturated value when the thickness exceeds ~100 nm. **Figure 4** presents the enlarged piezoelectric properties d_{33} of few-layer In_2Se_3 on different substrates (Pt, *p*-type Si and *n*-type Si substrates). The piezoelectric coefficient d_{33} of In_2Se_3 on the Pt substrate ranges from 0.3 to 8.85 pm V^{-1}, producing the variation in the piezoelectric value of ~29.5. The definition of the piezoelectric change value is the ratio of the maximum value of piezoelectric coefficient/the minimum value of piezoelectric coefficient, which corresponds to $d_{33,max}/d_{33,min}$. The piezoelectric coefficient d_{33} of few-layer In_2Se_3 on the Si substrate is lower than that of In_2Se_3 on the Pt substrate, and the tunable piezoelectric coefficient d_{33} of In_2Se_3 on the *p*-type Si substrate changes from 0.014 to 9.19 pm V^{-1}, exhibiting the variation piezoelectric value of ~650. As comparison, the piezoelectric coefficient d_{33} of In_2Se_3 on the Au substrate is measured from 0.89 to 5.98 pm V^{-1} under the same experimental condition (Figures S12–S15, Supporting Information), showing a variation in the piezoelectric value of ~6.7, which is similar to the reported result.[13,17] It is noted that the piezoelectric coefficient d_{33} of In_2Se_3 on different substrates can be remarkably modulated by constructing diverse interfaces.

To understand the physical mechanism of tunable piezoelectric properties with interface engineering, we performed density functional theory (DFT) calculations on the electronic structural properties of In_2Se_3 samples. According to experimental result, we constructed the corresponding heterojunctions of In_2Se_3 with Pt and Si. **Figure 5** shows the fully optimized structures, where the interface distance of In_2Se_3 and the substrate are 2.24 and 2.36 Å in α-In_2Se_3/Pt (111) and α-In_2Se_3/Si (111), respectively. A vacuum layer of 20 Å along the *z*-axis is added to avoid the interaction of layers. To quantitively examine the amount of charge transfer, the plane-averaged differential charge density $\Delta\rho$ is calculated using $\Delta\rho = (\rho_{heterojuction} - \rho_{In_2Se_3} - \rho_{Pt/Si})/S$, where $\rho_{heterojuction}$, $\rho_{In_2Se_3}$ and $\rho_{Pt/Si}$ are the charges of α-In_2Se_3/Pt (111) and α-In_2Se_3/Si (111) heterojunctions, α-In_2Se_3 and Pt (111) or Si (111) layer, respectively. The differential charge density and corresponding plane-averaged differential charge density in z direction shown in **Figure 6** are used to evaluate the interlayer charge transfer in α-In_2Se_3/Pt (111) and α-In_2Se_3/Si (111) heterojunctions. From the differential charge density distribution diagram (Figure 6a,b), it is obviously that the interlayer charge transfer in the α-In_2Se_3/Pt (111) is stronger than that of α-In_2Se_3/Si (111). Besides, the shorter interlayer distance in α-In_2Se_3/Pt (111) heterojunction indicates that the stronger coupling than α-In_2Se_3/Si (111) heterojunction. To further quantitatively evaluate the strength of charge transfer between layers, we integrated the plane-averaged differential charge density of In_2Se_3 layer along the z direction (Figure 6c,d). The integral results show that the amount of transferred charge move from α-In_2Se_3 to Pt (111) layer is ~0.57 e^- in α-In_2Se_3/Pt (111) heterojunction. Different from the α-In_2Se_3/Pt (111) heterojunction, the direction

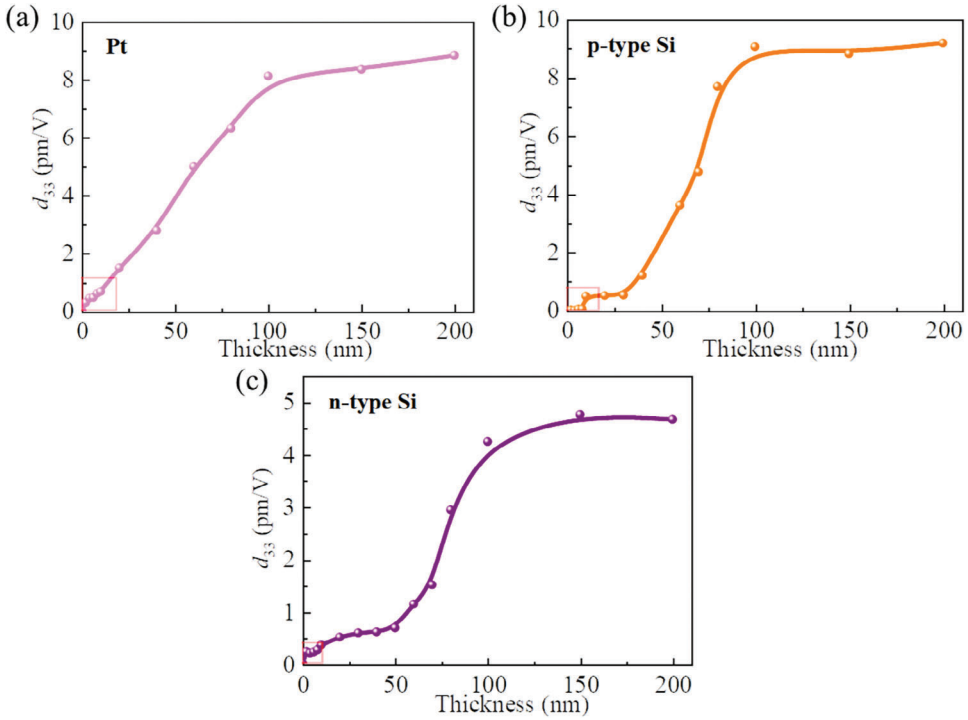

Figure 3. Thickness-dependent piezoelectric properties d_{33} of α-In_2Se_3 onto different substrates: a) Pt; b) *p*-type Si; c) *n*-type Si.

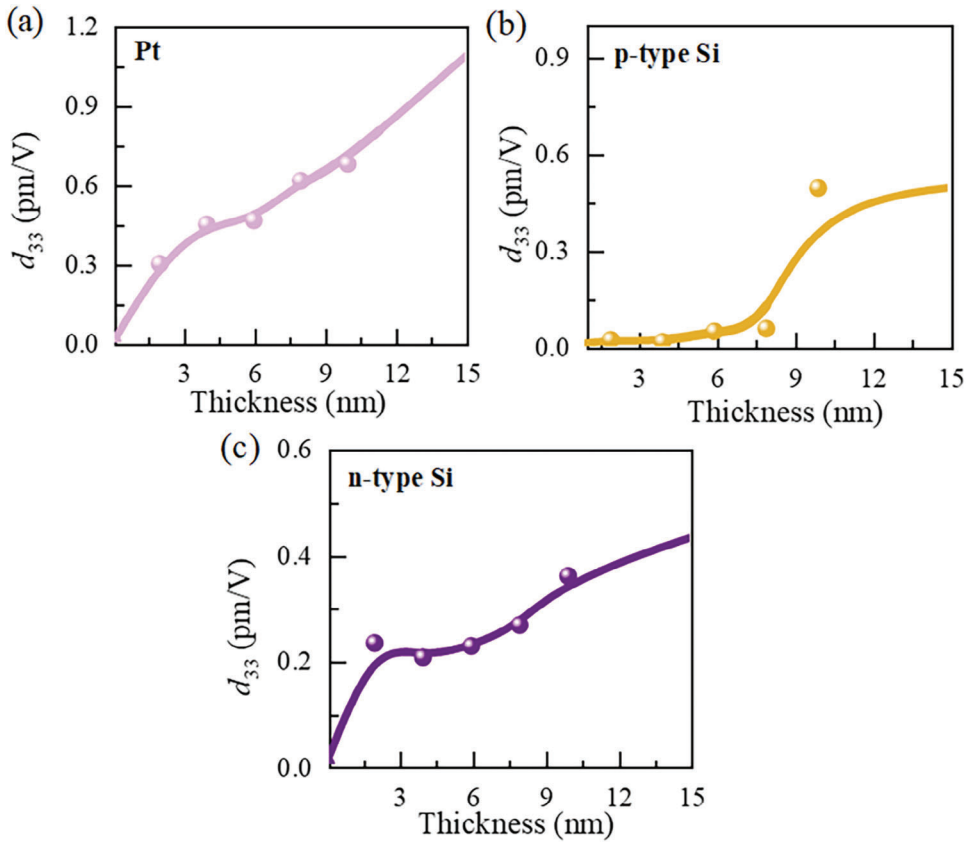

Figure 4. Thickness-dependent piezoelectric properties d_{33} of few-layer α-In_2Se_3 onto different substrates: a) Pt; b) *p*-type Si; c) *n*-type Si.

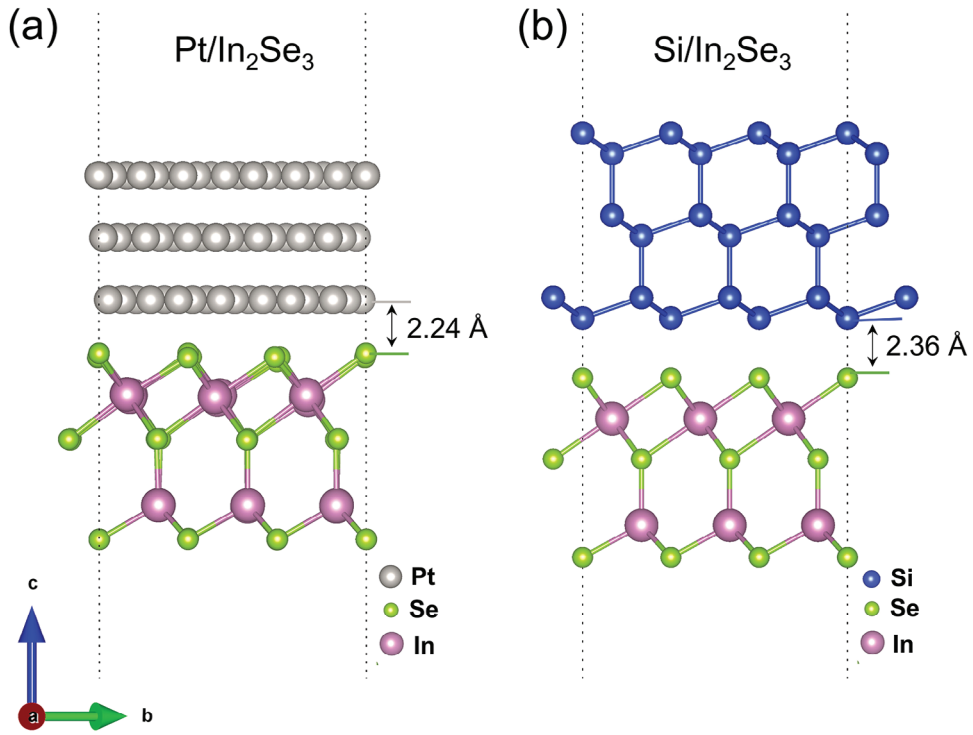

Figure 5. The optimized structures of a) α-In_2Se_3/Pt (111) and b) α-In_2Se_3/Si (111) heterojunctions. The orange, purple, green, and blue balls represent Pt, In, Se and Si atoms, respectively.

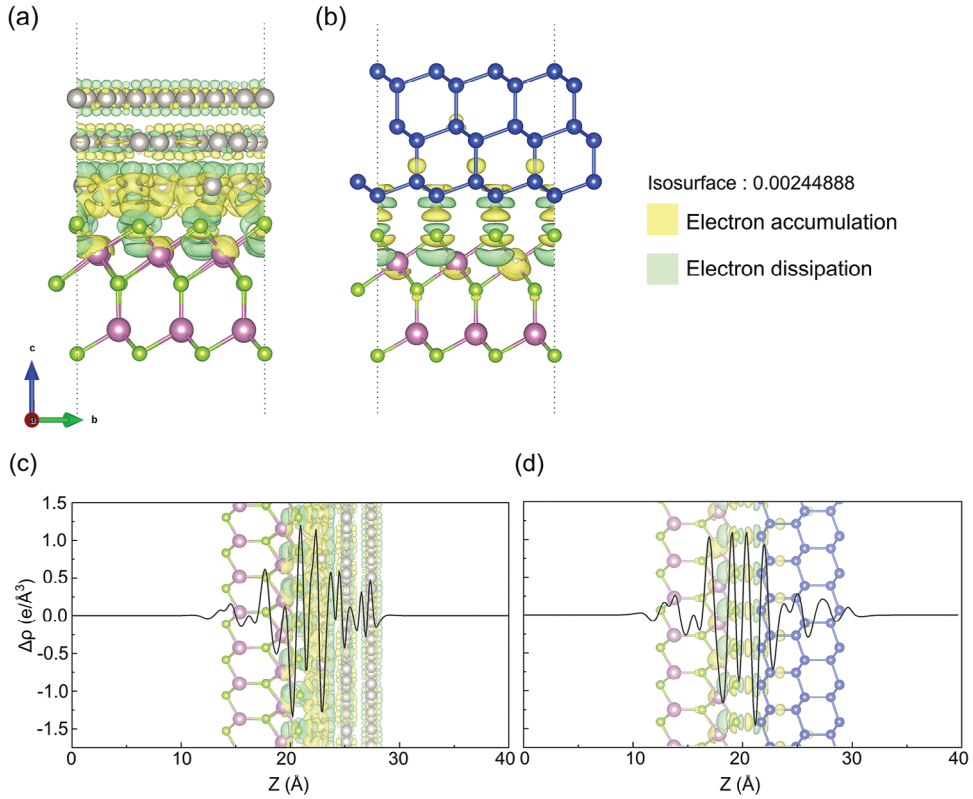

Figure 6. Differential charge density distribution with an isosurface 0.002 e/bohr^3 of a) α-In_2Se_3/Pt (111) and b) α-In_2Se_3/Si (111) heterojunctions. The yellow (or green) bubbles denote the accumulation (or dissipation) of electrons. The corresponding plane-averaged differential charge density in z-direction is shown in (c) and (d).

of charge transfer in α-In_2Se_3/Si (111) heterojunction is from Si (111) layer to α-In_2Se_3 and the amount of transferred charge is ~0.14 e^- which is smaller than α-In_2Se_3/Pt (111) heterojunction. According to our previous result, the charge transfer between ferroelectric In_2Se_3 and semiconducting layer can form the additional interfacial dipole moment, leading to the enhancement of out-of-plane piezoelectric properties.[17,21] The charge transfer in α-In_2Se_3/Si (111) heterojunction is smaller than that of α-In_2Se_3/Pt (111) heterojunction, which corresponds the piezoelectric coefficient d_{33} of α-In_2Se_3 onto Si substrate is than that of α-In_2Se_3 onto Pt substrate. The different charge transfer phenomenon in two heterojunctions is well consistent with the experimental result.

The piezoelectric properties of 2D materials can be manipulated in terms of strain, thickness, elemental substitution, and defect engineering approaches. However, the tunable piezoelectric properties of 2D materials are difficult to achieve through these methods. Typically, the variation in the piezoelectric value of 2D materials via the thickness difference is approximately less than 20, such as In_2Se_3,[13] SnS_2,[18] InSe,[19,22] CdS,[20] WSe_2,[23] $CuInP_2S_6$,[24] and $NbOI_2$.[16] The variation piezoelectric value of 2D MoS_2 and $MoTe_2$ with defect modulation can only be changed by less than 2.[25,26] In addition, the tunable piezoelectric value of MoO_2 with defects from electret formation during synthesis is ~7.8.[27] According to DFT calculations, the out-of-plane piezoelectric coefficient d_{33} depends on the stacking sequence in multilayer MoSTe,[28] and the variation piezoelectric value is ~2.4. The 2D materials can also stack with similar 2D layers to form heterostructures, in which their piezoelectric properties are larger than that of the individual materials,[17,29,30] for instance In_2Se_3/MoS_2, In_2Se_3/WS_2, and SnS_2/SnS, but the variation in the piezoelectric value is still lower than 10. Using DFT calculations, the MoSeTe/WSTe heterostructure can be controlled in a stacking order-dependent manner, and the tunable value is also ~2.5 for multilayer Janus structures of transition metal dichalcogenides.[31] Recently, vertical piezoelectricity and ferroelectricity are found in untwisted MoS_2/WS_2 heterostructure by chemical vapor deposition growth. The piezoelectric performance is varied from 1.95 to 2.09 pm V^{-1} through modulating the phase from 2H-like to 3R-like MoS_2/WS_2 heterostructure, and the tunable value of piezoelectric properties is also less than 2.[2] In typical perovskite oxide, the tuning d_{33} value of deformed $BaTiO_3$ sample was a factor of ~19 times compared with the undeformed referred sample.[32] Therefore, the variation in the piezoelectric properties via these methods is limited by one order of magnitude. In this work, we can significantly modulate the piezoelectric properties of 2D materials In_2Se_3 via interface engineering. The variation value of piezoelectric properties d_{33} is ~650, which demonstrates the highest variation value in the 2D piezoelectric materials system, as shown in **Figure 7**. More importantly, the In_2Se_3 samples are fabricated onto silicon substrates, which are compatible with silicon semiconductor technologies. In addition, the variation value of piezoelectric properties d_{33} onto different substrates display distinguishable change, which is able to use for detecting the carrier doping type such *p*-type, *n*-type semiconductor and metal. The unprecedented tunable piezoelectric properties make 2D materials highly attractive for advanced piezoelectric applications that include pressure sensing, piezocatalysis, piezotronics, and energy harvesting.

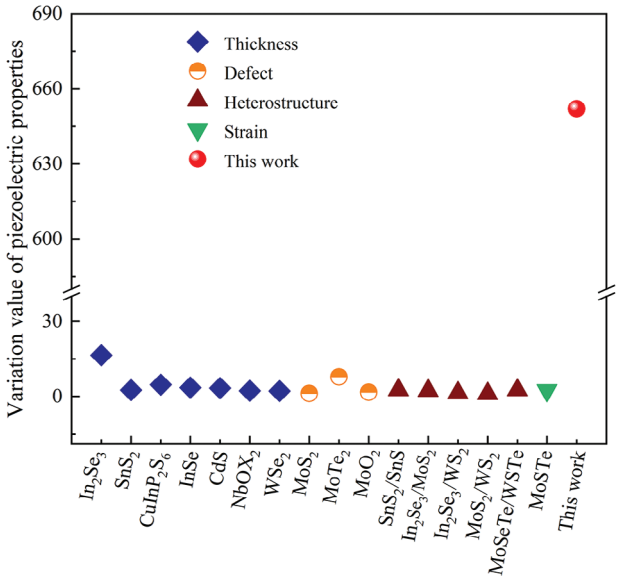

Figure 7. Comparison of tunable piezoelectric performance of 2D materials.

3. Conclusion

In summary, we have demonstrated a giant tunable piezoelectric coefficient d_{33} for 2D layered piezoelectric materials In_2Se_3 via interface modulation. An out-of-plane variation piezoelectric value of In_2Se_3 is around 650, exhibiting the ultrahigh variation value in the 2D piezoelectric materials system. In addition, 2D piezoelectric materials can be directly fabricated onto silicon substrate, which is compatible with silicon technology. Combining the DFT calculation, the giant variation piezoelectric value is attributed to the charge transfer of the interface. As a result, our study opens an alternative approach in designing and manipulating novel smart and multifunctional devices.

4. Experimental Section

Preparation and Characterization of In_2Se_3 Samples: The In_2Se_3 nanoflakes were fabricated using mechanical exfoliation method with scotch tape. Raman spectroscopy was used to determine the sample's Raman spectrum. With the aid of transmission electron microscope equipped with energy dispersive X-ray (EDX) analysis (JEOL JEM-2100), microstructures and chemical compositions were studied. On a commercial atomic force microscope (Asylum Research MFP-3D), PFM measurements were performed, and a tip was applied by an ac voltage (V_{ac} = 0.5~3 V). Using the dual AC resonance tracking (DART) mode, PFM images were captured. In dual frequency resonance tracking mode, piezoresponse loops were gathered.

DFT Calculations: The heterojunctions optimization and electronic structure calculations were performed using Vienna ab initio simulation package (VASP) based on density functional theory (DFT).[33,34] The exchange-correlation functional was described by generalized gradient approximation (GGA) within the framework of Perdew-Burke-Ernzerhof (PBE).[35] The atomic forces were less than 0.001 eV $Å^{-1}$ during the structural relaxations and the electronic energy convergence criteria was set to be 10^{-6} eV in electronic self-consistent calculation. The energy cutoff was set to 400 eV for the plane-wave basis expansion and the Γ-centered k-point sampling was set to 5 × 5 × 1 and 7 × 7 × 1 for two different

heterojunctions. The van der Waals (vdW) interactions of heterojunctions were taken into consideration by the DFT-D3 method.[36] To minimize the lattice mismatch, it choose $2\sqrt{5} \times 2\sqrt{5}$ Pt (111) with the 3×3 α-In_2Se_3 unit cell and 3×3 Si (111) unit cell with 3×3 α-In_2Se_3 to build the α-In_2Se_3/Pt (111) and α-In_2Se_3/Si (111) heterojunctions, respectively. This study used a N atomic to substituted doping the 3×3 Si (111) to match the actual experiment.

Supporting Information

Supporting Information is available from the Wiley Online Library or from the author.

Acknowledgements

This work was supported by National Natural Science Foundation of China (Nos. 12175191, 11872054), Guangdong Basic and Applied Basic Research Foundation (Nos. 2022A1515110528, 2023A1515012792), New Faculty Startup Fund of China University of Geosciences (No. 162301212607), Guangdong Provincial Key Laboratory of Magnetoelectric Physics and Devices (No. 2022B1212010008), Natural Science Foundation of Hunan Province (Nos. 2022JJ30566, 2020JJ2026).

Conflict of Interest

The authors declare no conflict of interest.

Data Availability Statement

The data that support the findings of this study are available from the corresponding author upon reasonable request.

Keywords

2D materials, indium selenide, interface engineering, piezoelectric properties

Received: October 24, 2023
Published online: November 27, 2023

[1] P. C. Sherrell, M. Fronzi, N. A. Shepelin, A. Corletto, D. A. Winkler, M. Ford, J. G. Shapter, A. V. Ellis, *Chem. Soc. Rev.* **2022**, *51*, 650.
[2] L. Rogée, L. Wang, Y. Zhang, S. Cai, P. Wang, M. Chhowalla, W. Ji, S. P. Lau, *Science* **2022**, *376*, 973.
[3] M.-M. Yang, Z.-D. Luo, Z. Mi, J. Zhao, S. P. E, M. Alexe, *Nature* **2020**, *584*, 377.
[4] Y. Dong, M.-M. Yang, M. Yoshii, S. Matsuoka, S. Kitamura, T. Hasegawa, N. Ogawa, T. Morimoto, T. Ideue, Y. Iwasa, *Nat. Nanotechnol.* **2023**, *18*, 36.
[5] H. Liu, X. Shi, Y. Yao, H. Luo, Q. Li, H. Huang, H. Qi, Y. Zhang, Y. Ren, S. D. Kelly, K. Roleder, J. C. Neuefeind, L.-Q. Chen, X. Xing, J. Chen, *Nat. Commun.* **2023**, *14*, 1007.
[6] S. Yuan, X. Luo, H. L. Chan, C. Xiao, Y. Dai, M. Xie, J. Hao, *Nat. Commun.* **2019**, *10*, 1775.
[7] L. Hackett, M. Miller, S. Weatherred, S. Arterburn, M. J. Storey, G. Peake, D. Dominguez, P. S. Finnegan, T. A. Friedmann, M. Eichenfield, *Nat. Electron.* **2023**, *6*, 76.
[8] W. Wu, L. Wang, Y. Li, F. Zhang, L. Lin, S. Niu, D. Chenet, X. Zhang, Y. Hao, T. F. Heinz, J. Hone, Z. L. Wang, *Nature* **2014**, *514*, 470.
[9] Q. Zhang, S. Zuo, P. Chen, C. Pan, *InfoMat* **2021**, *3*, 987.
[10] K. Datta, Z. Li, Z. Lyu, P. B. Deotare, *ACS Nano* **2021**, *15*, 12334.
[11] H. Khan, N. Mahmood, A. Zavabeti, A. Elbourne, M. A. Rahman, B. Y. Zhang, V. Krishnamurthi, P. Atkin, M. B. Ghasemian, J. Yang, G. Zheng, A. R. Ravindran, S. Walia, L. Wang, S. P. Russo, T. Daeneke, Y. Li, K. Kalantar-Zadeh, *Nat. Commun.* **2020**, *11*, 3449.
[12] D. Tan, C. Jiang, N. Sun, J. Huang, Z. Zhang, Q. Zhang, J. Bu, S. Bi, Q. Guo, J. Song, *Nano Energy* **2021**, *90*, 106528.
[13] F. Xue, J. Zhang, W. Hu, W.-T. Hsu, A. Han, S.-F. Leung, J.-K. Huang, Y. Wan, S. Liu, J. Zhang, J.-H. He, W.-H. Chang, Z. L. Wang, X. Zhang, L.-J. Li, *ACS Nano* **2018**, *12*, 4976.
[14] A.-Y. Lu, H. Zhu, J. Xiao, C.-P. Chuu, Y. Han, M.-H. Chiu, C.-C. Cheng, C.-W. Yang, K.-H. Wei, Y. Yang, Y. Wang, D. Sokaras, D. Nordlund, P. Yang, D. A. Muller, M.-Y. Chou, X. Zhang, L.-J. Li, *Nat. Nanotech.* **2017**, *12*, 744.
[15] X. Jiang, X. Zhang, R. Niu, Q. Ren, X. Chen, G. Du, Y. Chen, X. Wang, G. Tang, J. Lu, X. Wang, J. Hong, *Adv. Funct. Mater.* **2023**, *33*, 2213561.
[16] Y. Wu, I. Abdelwahab, K. C. Kwon, I. Verzhbitskiy, L. Wang, W. H. Liew, K. Yao, G. Eda, K. P. Loh, L. Shen, S. Y. Quek, *Nat. Commun.* **2022**, *13*, 1884.
[17] S. Yuan, W. F. Io, J. Mao, Y. Chen, X. Luo, J. Hao, *ACS Appl. Nano Mater.* **2020**, *3*, 11979.
[18] Y. Wang, L.-M. Vu, T. Lu, C. Xu, Y. Liu, J. Z. Ou, Y. Li, *ACS Appl. Mater. Interfaces* **2020**, *12*, 51662.
[19] M. Dai, Z. Wang, F. Wang, Y. Qiu, J. Zhang, C.-Y. Xu, T. Zhai, W. Cao, Y. Fu, D. Jia, Y. Zhou, P.-A. Hu, *Nano Lett.* **2019**, *19*, 5410.
[20] X. Wang, X. He, H. Zhu, L. Sun, W. Fu, X. Wang, L. C. Hoong, H. Wang, Q. Zeng, W. Zhao, J. Wei, Z. Jin, Z. Shen, J. Liu, T. Zhang, Z. Liu, *Sci. Adv.* **2016**, *2*, 1600209.
[21] Y. Chen, Z. Tang, H. Shan, B. Jiang, Y. Ding, X. Luo, Y. Zheng, *Phys. Rev. B* **2021**, *104*, 075449.
[22] F. Sui, M. Jin, Y. Zhang, R. Qi, Y.-N. Wu, R. Huang, F. Yue, J. Chu, *Nat. Commun.* **2023**, *14*, 36.
[23] J.-H. Lee, J. Y. Park, E. B. Cho, T. Y. Kim, S. A. Han, T.-H. Kim, Y. Liu, S. K. Kim, C. J. Roh, H.-J. Yoon, H. Ryu, W. Seung, J. S. Lee, J. Lee, S.-W. Kim, *Adv. Mater.* **2017**, *29*, 1606667.
[24] W. F. Io, M.-C. Wong, S.-Y. Pang, Y. Zhao, R. Ding, F. Guo, J. Hao, *Nano Energy* **2022**, *99*, 107371.
[25] S. A. Han, T.-H. Kim, S. K. Kim, K. H. Lee, H.-J. Park, J.-H. Lee, S.-W. Kim, *Adv. Mater.* **2018**, *30*, 1800342.
[26] S. Kang, S. Kim, S. Jeon, W.-S. Jang, D. Seol, Y.-M. Kim, J. Lee, H. Yang, Y. Kim, *Nano Energy* **2019**, *58*, 57.
[27] A. Apte, K. Mozaffari, F. S. Samghabadi, J. A. Hachtel, L. Chang, S. Susarla, J. C. Idrobo, D. C. Moore, N. R. Glavin, D. Litvinov, P. Sharma, A. B. Puthirath, P. M. Ajayan, *Adv. Mater.* **2020**, *32*, 2000006.
[28] L. Dong, J. Lou, V. B. Shenoy, *ACS Nano* **2017**, *11*, 8242.
[29] V. A. Cao, M. Kim, W. Hu, S. Lee, S. Youn, J. Chang, H. S. Chang, J. Nah, *ACS Nano* **2021**, *15*, 10428.
[30] C. W. Jang, H. Kim, M. K. Nazeeruddin, D. H. Shin, S.-H. Choi, *Nano Energy* **2021**, *84*, 105899.
[31] A. Rawat, M. K. Mohanta, N. Jena, Dimple, R. Ahammed, A. De Sarkar, *J. Phys. Chem. C* **2020**, *124*, 10385.
[32] M. Höfling, X. Zhou, L. M. Riemer, E. Bruder, B. Liu, L. Zhou, P. B. Groszewicz, F. Zhuo, B.-X. Xu, K. Durst, X. Tan, D. Damjanovic, J. Koruza, J. Rödel, *Science* **2021**, *372*, 961.
[33] P. E. Blöchl, *Phys. Rev. B* **1994**, *50*, 17953.
[34] G. Kresse, D. Joubert, *Phys. Rev. B* **1999**, *59*, 1758.
[35] J. P. Perdew, K. Burke, M. Ernzerhof, *Phys. Rev. Lett.* **1996**, *77*, 3865.
[36] S. Grimme, J. Antony, S. Ehrlich, H. Krieg, *J. Chem. Phys.* **2010**, *132*, 154104.